

The use of time-of-flight static secondary ion mass spectrometry imaging for the molecular characterization of single aerosol surfaces

Rita Van Ham^a, Annemie Adriaens^{b,*}, Luc Van Vaeck^a, Freddy Adams^a

^a University of Antwerp, Department of Chemistry, Universiteitsplein 1, B 2610 Antwerp, Belgium

^b Ghent University, Department of Analytical Chemistry, Krijgslaan 281-S12, B 9000 Ghent, Belgium

Received 7 July 2005; received in revised form 31 October 2005; accepted 10 November 2005

Available online 6 January 2006

Abstract

The imaging feasibility of time-of-flight static secondary ion mass spectrometry (TOF S-SIMS) has been investigated for the identification of the molecular composition of inorganic constituents at the surface of single aerosol particles. Selected test cases involved the study of single ambient aerosol particles (aerodynamic diameter 2–4 μm) collected by cascade impaction and the characterization of laboratory made CaCO_3 particles exposed to HNO_3 and H_2SO_4 . A methodological optimization of the experiments helped in identifying a proper collection substrate (silicon wafer), the use of a low particle loading and the application of sputter pre-cleaning as essential aspects to record high quality secondary ion images of molecule specific adduct ions (i.e. one or more analyte molecules attached to a stable ion). Correlation of the features in the ion images at different m/z and the knowledge about the systematic trends in the formation of structural ions from inorganic salts allowed the identification of the molecular composition of the constituents in the studied particles.

© 2005 Elsevier B.V. All rights reserved.

Keywords: Aerosols; Speciation; Imaging; Surface analysis; TOF S-SIMS

1. Introduction

Aerosol particles are ubiquitous throughout the atmosphere and have a significant impact on diverse aspects of our biosphere. The direct effect on human health relates to the inhalation and deposition of aerosols allowing their toxic components to be taken up by the respiratory tissues. Suspended material also plays a role in the global warming since sub- μm particles are believed to scatter the sunlight and thereby counteract the greenhouse effect. A polluted atmosphere is a complex environment, where many reactive species interact in often photochemical processes. Understanding of the heterogeneous chemistry becomes a key-issue to obtain insight in the atmospheric self-cleaning and pollution processes.

Aerosols comprise suspended material in an extremely broad size range, i.e. from 1 to 100 μm . Particles within the different size sub-ranges show a large variation in physical and chemical properties. The so-called accumulation mode (particles between

0.1 and 2.5 μm) contains the maximum of the surface distribution, which is important for the heterogeneous chemistry, and represents toxicologically the most dangerous fraction because of retention deep in the respiratory tract. Chemical analysis is required not only at the level of single particles but also distinction between the ultimate surface layer and the bulk composition is needed to assess e.g. the source and history of the particle, and to get insight in the atmospheric processes. Furthermore, large populations of individual particles must be studied in order to obtain a representative picture of the aerosol in the atmosphere.

Accumulation mode particles fit within the lateral resolution capabilities of current microprobes. Off-line analysis of size fractionated aerosols is traditionally performed with scanning electron microscopy (SEM), electron probe micro-analysis (EPMA) and particle induced X-ray analysis (PIXE) [1–5]. Additionally, X-ray photoelectron spectroscopy (XPS) [6] and micro-Raman or infrared spectrometry [7,8] are used for bond-specific data whereas time of flight laser microprobe mass spectrometry (TOF LMMS) has been the first method to perform molecular speciation in single particles [9–13].

Off-line methods, however, are inherently handicapped by the sampling procedure. Apart from the reduced time resolution,

* Corresponding author. Tel.: +32 9 264 48 26.

E-mail address: annemie.adriaens@ugent.be (A. Adriaens).

exposure of the collected aerosol to massive amounts of air during sampling can cause volatilisation, hydration and chemical reactions. Therefore, particle beam interfaces have been developed for the direct introduction of suspended aerosols in the vacuum chamber of the MS, allowing on-line analysis of single particles to be achieved [14–16]. Light scattering is used to trace back the presence of a single particle within a given size range in the waist of the ionising laser. A dual TOF MS allows positive and negative ion mass spectra to be recorded from the same particle [17]. Such aerosol TOF MS (ATOFMS) instruments have now sufficiently matured for field applications to emission and ambient aerosol monitoring [18–20].

Nevertheless a real-time MS gives little morphological information (shape of the particle), while the evaporation of the entire particle at once prevents distinction between the composition of the surface layer and the bulk. In this respect, static secondary ion mass spectrometry potentially offers advantageous capabilities such as imaging, molecular information about inorganic components in the outer surface monolayer and detailed morphological examination by secondary electron images in the same instrument.

The breakthrough of TOF S-SIMS in material analysis [21–23] has motivated us to explore its application to single environmental particles mainly because of some potentially interesting capabilities. First, the lateral resolution is in the μm range or better [24] and the detection limits of TOF S-SIMS have been demonstrated to be within the range of requirements for environmental applications, at least as far as the elemental composition is to be characterized (in the order of 10^9 atoms cm^{-2}) [25]. Second, TOF S-SIMS has been proved to yield highly specific adduct ions for the molecular speciation of inorganic compounds, at least in the case of pure analytes [26–34]. Third, the information depth is essentially one monolayer, causing the detected signals to refer uniquely to the surface components, which is useful when for instance when studying the exchange of blood and surface components after inhalation. Additionally, there is the possibility to image secondary adduct ions with a lateral resolution which depend primarily on the ion yield [35]. Finally, secondary electrons generated by primary ion impact allow detailed morphological examination with a resolution between that of a light microscope and dedicated electron microprobes. So far, only a very few attempts have been made on aerosols [36–39].

The purpose of this paper is to report on the feasibility of TOF S-SIMS imaging for the characterization of aerosols by means of molecular information. Experiments have been performed on single ambient aerosol particles in the 2–4 μm size range and calcite model systems exposed to acidic atmospheres.

2. Experimental

2.1. Samples

Size fractionated ambient aerosols were collected on the university campus (Antwerp) with a Berner impactor. As to particle collection substrates aluminium foil, indium foil, and silicon wafer were considered because of their flatness and conductiv-

ity so that charging of the samples during analysis would cause not any significant problem. Experiments, however, showed that the chemical reactivity of aluminium and indium foils towards various salts (LiCl, CuCl, NaCl, KCl, NaBr, KBr, NaI, and KI) made these substrates inadequate. All salts except KCl and NaCl readily attacked aluminium. Black spots (redox reactions) were already formed before the sample preparation was finished. NaI and LiCl only reacted after a few days or weeks. The same problem existed with the indium foil, commonly used as substrate in SIMS experiments. Therefore a silicon wafer was preferred as the collection substrate, which was not visibly damaged by any of the salts. In addition not any signals pointing to analyte-substrate reactions could be detected.

The silicon wafer was cut into small pieces (10 mm \times 7 mm) matching the S-SIMS sample holder. To ensure proper functioning of the impactor, the substrate surface is to be mounted flush with the original sample stage. Therefore the Berner impaction plate was modified so that untreated silicon wafer samples could be attached by double-sided tape without disturbing the airflow (Fig. 1). The advantages of this sample preparation were that the coverage of aerosols on the substrate occurred in small spots, which were relatively flat, and that the surface coverage could be easily controlled by the collection time.

Samples were collected at a flow rate of 25 L min^{-1} for ca. 90 min. The collection time was chosen to keep the impacted particles well separated on the substrate. Not any additional sticking medium to reduce bounce-off or blow-off was applied. The particle fractions 2–4 and 4–8 μm (aerodynamic diameter) were used for analysis.

The second set of experiments involved spraying an aqueous suspension of CaCO_3 with an airbrush (Badger, IL) under a pressure of about 1 bar, adjusted for a spray diameter of 1 cm at a distance of 5 cm. The micro-droplets were dried by transfer through a tube (length 40 cm, diameter 1.5 cm) under a nitrogen stream of 26 L min^{-1} . Particles of 2–4 μm were collected for about 10 min with a Berner cascade impactor using silicon wafer collection substrates. The loaded substrate was exposed to an atmosphere saturated with HNO_3 or H_2SO_4 during 5 min up to 2 and 48 h, respectively.

2.2. Instrumentation

Analyses were performed with a TOF S-SIMS IV (ION-TOF, Germany) instrument using a Ga^+ liquid metal ion gun (LMIG). The Ga^+ pulse was bunched to 20–40 ns for the imaging experiments. Although the “collimated mode” yields a smaller beam spot (and a better lateral resolution), the “crossover mode” was preferred to obtain a sufficient number of secondary ions in a reasonable time. Images were recorded from raster areas between 60 $\mu\text{m} \times 60 \mu\text{m}$ and 220 $\mu\text{m} \times 220 \mu\text{m}$ depending on the particle size. Full spectra were stored for each of the 128 \times 128 pixels. Each pixel was bombarded with 32 pulses per pixel per scan and scans were accumulated were necessary.

2.3. Applied ion dose

The applied ion dose was of the order of 10^{11} ions cm^{-2} . As it could vary from one experiment to another, it is indicated in

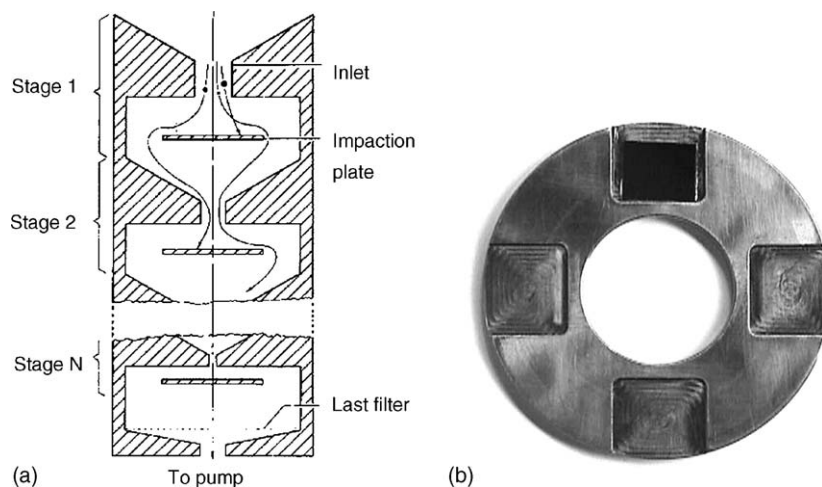


Fig. 1. Experimental set-up for the collection of aerosols: (a) schematic diagram of a Berner impactor; (b) impaction plate of the Berner impactor modified to hold silicon substrates.

each of the figure captions. A static regime (i.e. total number of primary ions equals current density multiplied by time, must be kept under a given static limit) is needed to fully exploit the molecular capabilities in imaging. However, the direct determination of the damage cross-section (i.e. the rate of signal decay with ion dose), which may be matrix-dependent, is very difficult to achieve in single particle analysis. The practical solution consists in superimposing consecutively recorded images from the same field. Fig. 2a depicts the ion intensity as a function of the irradiation dose or scan number for a NaBr particle, impacted on silicon substrate after aerosol spraying.

It has been observed that the intensity per scan for NaBr-Br⁻ stays constant (125 ± 11 counts per scan). The relative standard deviation corresponds to the expected precision. Hence, the additional ion doses still add significant contributions to the finally detected molecular ion signal. The software addition of

successive scans provides a rapid and simple but qualitative way to assess the same effect. Fig. 2b shows that the gain in image intensity and quality for NaBr-Br⁻ after five scans equals that of Br⁻, which suggests that the static regime is applied. Note that this experiment has been performed on a homogeneous particle.

2.4. Pre-cleaning of the samples

Imaging of inorganic speciation information also requires pre-cleaning of the surface by rastering the primary beam in the direct current mode over an area of four times the selected region of interest during two to three scans. This pre-cleaning is needed as the surface of the collected aerosols is covered by water, which must be removed before the information of interest can be detected. Figs. 3 and 4 illustrate consecutively measured ion images from outdoor aerosols collected on silicon. The very

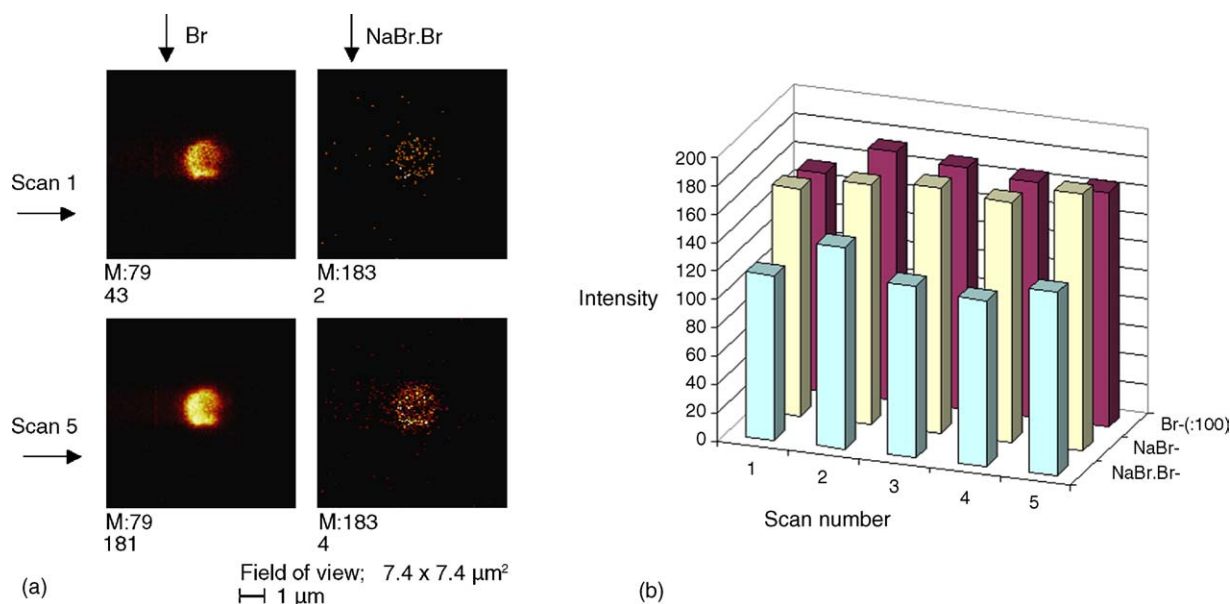



Fig. 2. (a) The ion intensity as a function of the irradiation dose or scan number for a NaBr particle, impacted on silicon substrate after aerosol spraying. (b) The gain in image intensity and quality for NaBr-Br⁻ after five scans.

File: IST7NA.MIF
Pulses/Pixel: 64

Field of view: 218 x 218 μm^2
 50 μm

Scans: 1-4

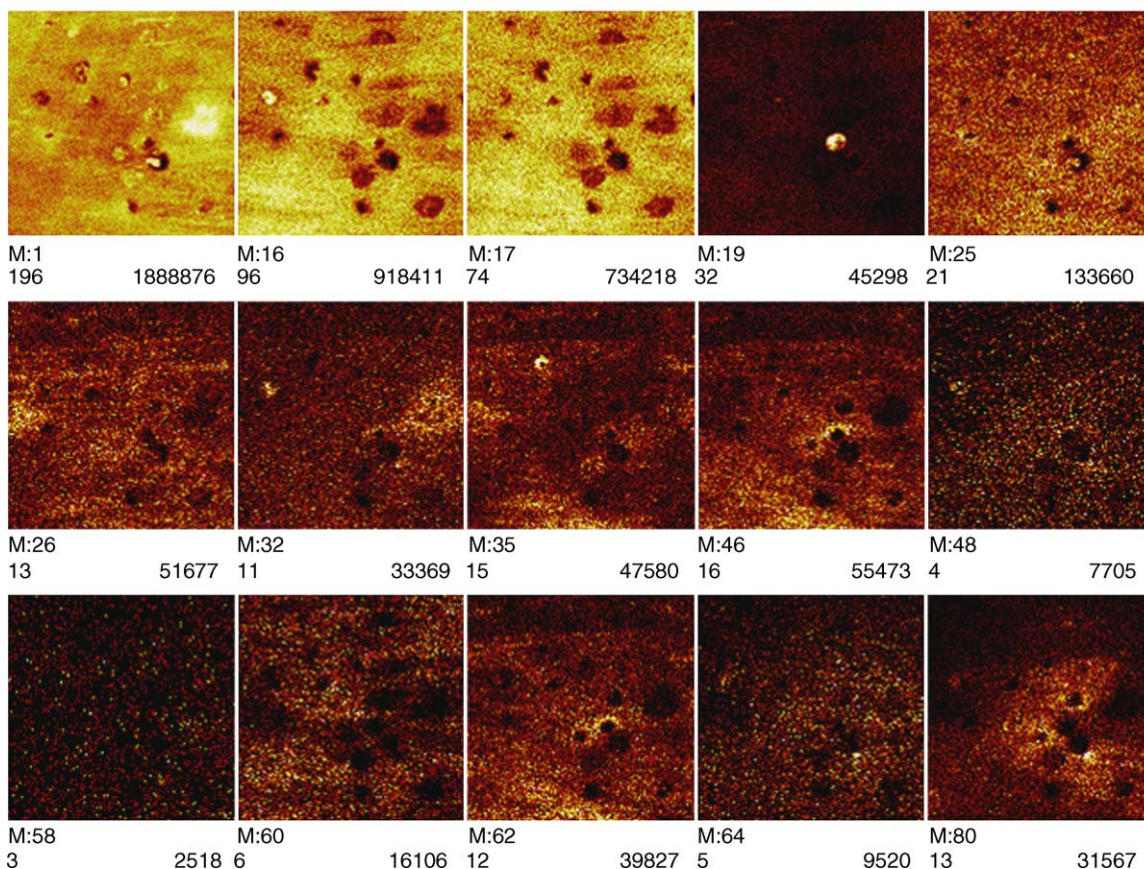


Fig. 3. Secondary ion images from ambient aerosol particles on a silicon collection substrate, recorded before sputter cleaning. The totally applied ion dose was 1.7×10^{10} ions cm^{-2} . The notation M refers to the m/z of H^- (m/z 1), O^- (m/z 16), OH^- (m/z 17), F^- (m/z 19), C_2H^- (m/z 25), CN^- (m/z 26), $\text{O}_2^- + \text{S}^-$ (m/z 32), Cl^- (m/z 35), NO_2^- (m/z 46), SO^- (m/z 48), CNS^- (m/z 58), SiO_2^- (m/z 60), NO_3^- (m/z 62), SO_2^- (m/z 64) and SO_3^- (m/z 80).

first scans, shown in Fig. 3, only yield information about the surface coverage by H^- , O^- and OH^- , as well as on a single particle with high F^- yield. In general (except for hydrated components present at the surface), the OH^- image directly characterizes the uncovered substrate where the particles appear as less intense spots. This “complementary” information on the particle localization is less clear in the images. After pre-cleaning (Fig. 4), a completely different picture is obtained. The background from the substrate is significantly reduced and the specific signals for the particle components yield clearly visible features. Specifically, most of the collected material can be associated with sulphate (S^- or O_2^- , SO^- , SO_2^- , SO_3^-) and nitrate (O_2^- , NO^- , NO_2^- , NO_3^-) aerosols, while the other particles point to organic or carbonaceous matter. Interestingly, Cl^- is detected in some sulphate particles, but not in the nitrate aerosols of this small population. Although the pre-cleaning step destroys the organic molecules in the outer layer, it does not prevent the detection of structural adduct ions from the underlying layer. Otherwise stated, the static ion dose, i.e. the number of primary ions that can impact on a given area before the generation of structural ions vanishes, is not exceeded by the sputter cleaning, at least for inorganic compounds.

Molecular adduct ion images often reach maximum intensities in the rather low range of 3–5 counts per pixel (typical background is 1 count per pixel), which can be considered as the limit of the S-SIMS technology. Therefore, the raster area must be selected in such a way that the particle of interest covers at least 40 pixels. On the other hand, the number of particles within an image must be restricted to about 10 particles by limiting the aerosol loading of the substrate. A population of e.g. 100 particles in a raster of $300 \mu\text{m} \times 300 \mu\text{m}$ hampers the distinction between particles and noise as the number of particles becomes too low. The use of more pixels per raster area increases the size of the raw data file drastically with detrimental effects of the processing efficiency later on.

3. Results and discussion

3.1. Characterization of single ambient aerosols by secondary ion images

One of the major advances in TOF S-SIMS against real-time A TOF MS is the complementing information that can be obtained from high-resolution secondary electron images. A

File: \ST7NA.MIF
Pulses/Pixel: 64Field of view: 218 x 218 μm^2
— 50 μm

Scans: 1-3

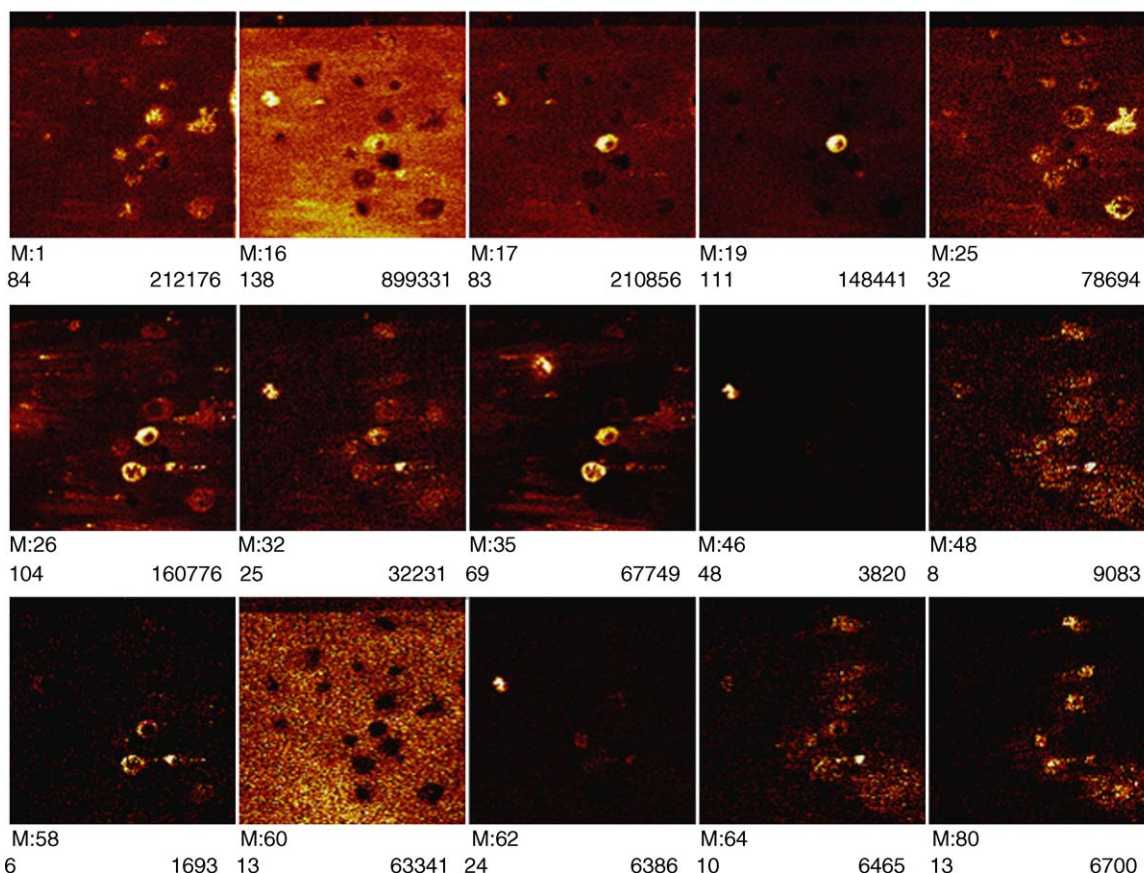


Fig. 4. Secondary ion images from the sample as in Fig. 3 after sputter cleaning. The notation M refers to the m/z of H^- (m/z 1), O^- (m/z 16), OH^- (m/z 17), F^- (m/z 19), C_2H^- (m/z 25), CN^- (m/z 26), $\text{O}_2^- + \text{S}^-$ (m/z 32), Cl^- (m/z 35), NO_2^- (m/z 46), SO^- (m/z 48), CNS^- (m/z 58), SiO_2^- (m/z 60), NO_3^- (m/z 62), SO_2^- (m/z 64) and SO_3^- (m/z 80).

low primary ion dose is needed to avoid charge build-up in large particles and loss of resolution. On the other hand, the virtue of panoramic registration of a full mass spectrum for each pixel in TOF S-SIMS gives the possibility to collect all the information in a so-called raw data file for subsequent processing after analysis. This is a significant advantage in comparison to e.g. quadrupole S-SIMS where practically only pre-selected m/z can be imaged.

However, the extraction of relevant information from the huge raw data files tends to become a major obstacle to the successful application of TOF S-SIMS in the field. In practice the use of multivariate statistical approaches is all but obvious because of the limited number of particles that can be imaged. Hence the processing starts with the selection of images on the basis of coincident features. Positive and negative ions of only 10 particles typically yield 150 images with significant features, from which the relevant information must be extracted by correlating the images of different m/z .

As an example, Figs. 5 and 6 show the secondary electron and selected secondary ion images of an ambient aerosol sample. The structural identification by the correlated images uses the following general guidelines:

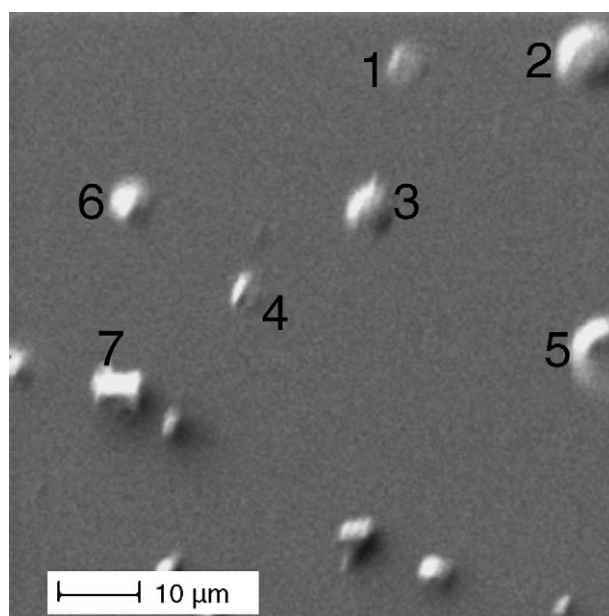


Fig. 5. Secondary electron image of the ambient aerosol particles studied (stage 6 of Berner impactor, size range 2–4 μm , collection Si wafer).

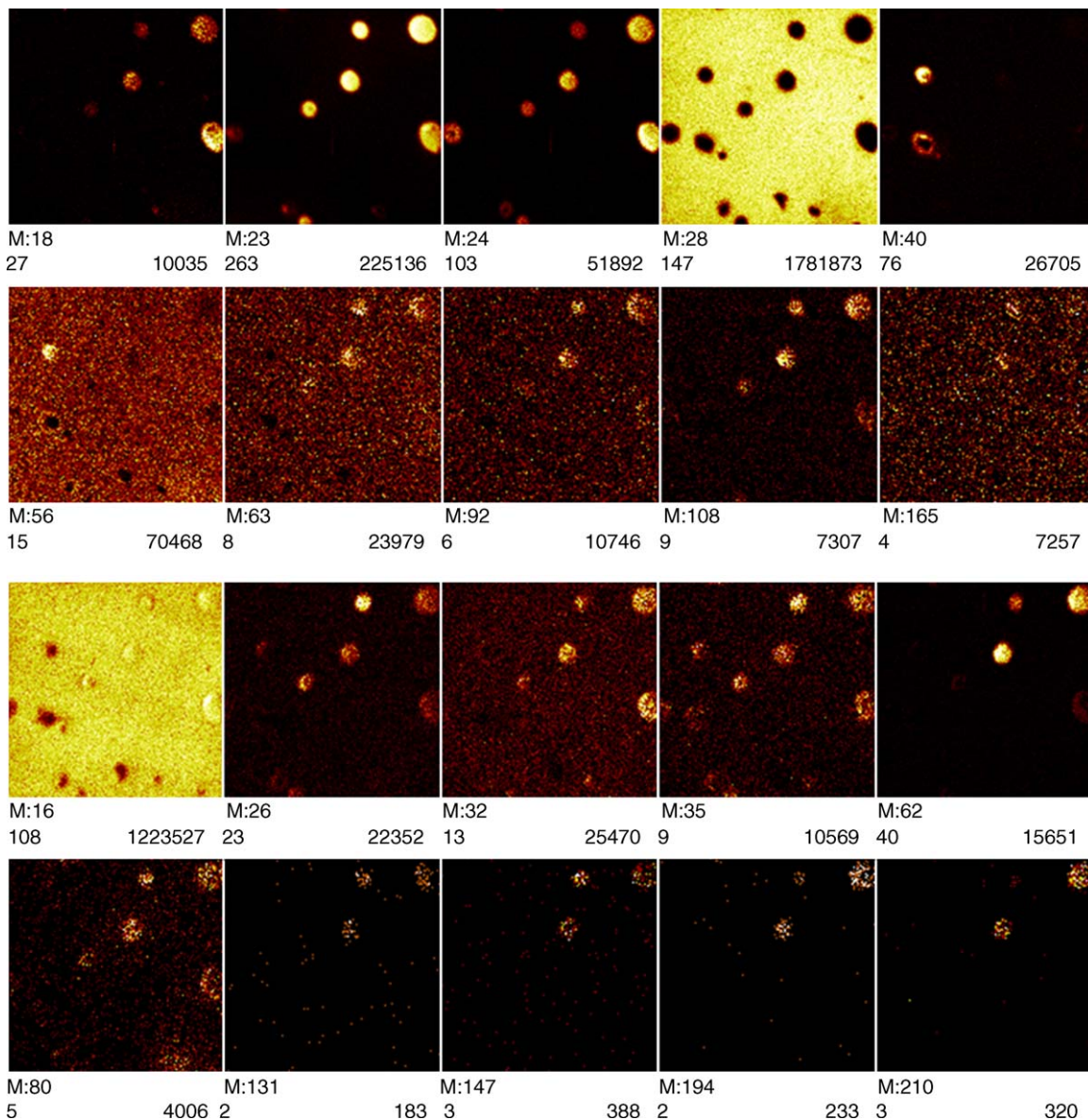


Fig. 6. Secondary ion images recorded from the ambient aerosol sample, shown in Fig. 3 in the positive (upper two series) and negative (lower two series) ion detection mode with a primary ion dose of 1.6×10^{11} ion cm^{-2} . The notation M refers to the m/z of NH_4^+ (m/z 18), Na^+ (m/z 23), Mg^+ (m/z 24), Si^+ (m/z 28), Ca^+ (m/z 40), CaO^+ (m/z 56), $\text{Na}_2\text{O}\cdot\text{H}^+$ (m/z 63), $\text{NaNO}_2\cdot\text{Na}^+$ (m/z 92), $\text{NaNO}_3\cdot\text{Na}^+$ (m/z 108) and $\text{Na}_2\text{SO}_4\cdot\text{Na}^+$ (m/z 165). Images for the negative ions are given for O^- (m/z 16), CN^- (m/z 26), $\text{O}_2^- + \text{S}^-$ (m/z 32), Cl^- (m/z 35), NO_3^- (m/z 62), SO_3^- (m/z 62), SO_3^- (m/z 80), $\text{NaNO}_3\cdot\text{NO}_2^-$ (m/z 131), $\text{NaNO}_3\cdot\text{NO}_3^-$ (m/z 147), $\text{Mg}(\text{NO}_3)_2\cdot\text{NO}_3^-$ (m/z 210).

- The Si^+ image (m/z 28) primarily serves to localize the particles (except for the quartz aerosols) after the pre-cleaning step.
- Data analysis starts with the images of elemental ions and low m/z fragment or cluster anions because of their intensity. These images already provide an indication of the possible building blocks to be considered for the high m/z (adduct) ion images. For instance, the positive ion mode shows a clear correlation between the Na^+ (m/z 23), Mg^+ (m/z 24) and NH_4^+ (m/z 18) for particles 1–5. Also the $\text{Na}_2\text{O}\cdot\text{H}^+$ image (m/z 63) exhibits the same trend which suggests the presence of oxysalts. Their identification as mainly sulphates and nitrates

comes from the SO_x^- (m/z 80) and NO_x^- (m/z 62) images. Confirmation of NaNO_3 or NaNO_2 as components of particles 1–3 is obtained from the images of the high m/z anions at m/z 147 ($\text{NaNO}_3\cdot\text{NO}_3^-$) and cations at m/z 108 ($\text{NaNO}_3\cdot\text{Na}^+$). No distinction between nitrate and nitrite could be made. The presence of Na_2SO_4 is traced back from the image at m/z 165 ($\text{Na}_2\text{SO}_4\cdot\text{Na}^+$) in the positive ion mode for particles 1–3 and 4–5. No adduct ions of the corresponding NH_4^+ analogues were detected. Finally, the magnesium salt is identified as $\text{Mg}(\text{NO}_3)_2$ by means of the anion images at m/z 194 and 210 (from $\text{Mg}(\text{NO}_3)_2\cdot\text{NO}_2^-$ and $\text{Mg}(\text{NO}_3)_2\cdot\text{NO}_3^-$, respectively) in particles 1–3.

- Although the ion images are recorded in low mass resolution, potential isobaric interferences can be dealt with, at least in part. For instance, the positive ions at m/z 56 can be due to Fe^+ or CaO^+ , but the relative intensities of the images for m/z 56 over 40 agrees with the ones observed for calcium oxysalts. Hence particle 6 is identified as a calcium salt.
- The correlation of the relative intensities in the ion images with the local concentration must be considered as purely qualitative. Since we are dealing with mixtures of components in the surface layers on matrices of unknown (and heterogeneous) composition, the ion yield of the analytes is likely to vary from particle to particle. Furthermore, the topography effects aggravate the situation. For instance, particle 7 shows a dark spot in the middle. No ions were detected from this spot. Hence, it can be due to the solvation effect [40]. A wet particle impacts and the water mantle dries in the vacuum, leaving a monolayer residue around the bulk particle. It is assumed that no ions are generated from this central thick particle because of composition or sample charging.
- Negative ions often give more intense signals and less background (organic contaminants) than cations. Therefore, data analysis is usually started with anions as the correlation of features becomes facilitated.

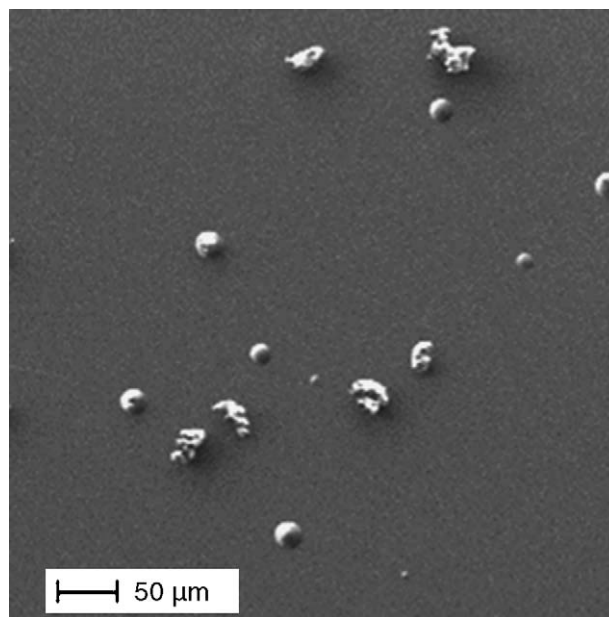


Fig. 7. Secondary electron image recorded with the TOF S-SIMS instrument of the studied CaCO_3 particles on a silicon wafer exposed to an atmosphere containing HNO_3 .

File: \26APNEA.MIF
Pulses/Pixel: 32

Field of view: 242 x 242 μm^2
50 μm

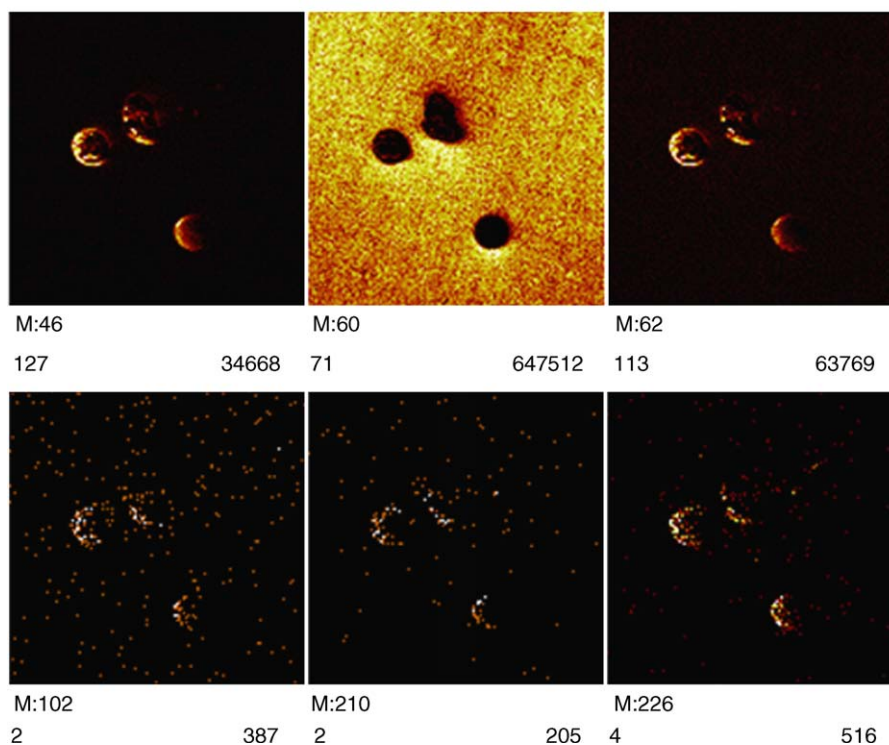


Fig. 8. Secondary ion images recorded from the sample shown in Fig. 7 using the negative ion detection mode and an ion dose of 7×10^{10} ion cm^{-2} . The notation M refers to the m/z of NO_2^- (m/z 46), NO_3^- (m/z 62), SiO_2^- (m/z 60), $\text{CaO}\cdot\text{NO}_2^-$ (m/z 102), $\text{Ca}(\text{NO}_3)_2\cdot\text{NO}_2^-$ (m/z 210) and $\text{Ca}(\text{NO}_3)_2\cdot\text{NO}_3^-$ (m/z 226). The data are summed over 20 scans.

3.2. Heterogeneous reactions at the surface of aerosols

The formation of secondary aerosol components is a key-issue in the understanding of the atmospheric processes in our environment. Heterogeneous chemistry of aerosols is not only intimately linked to the impact that dust has on the gas phase composition of the atmosphere, it can also influence how mineral dust aerosol impacts climate, biogeochemical cycles and health. For example, as mineral dust reacts in the atmosphere the physicochemical properties of the particles change including the optical properties of the particles and their effectiveness to serve as cloud condensation nuclei [41].

In this respect CaCO_3 particles (a major component of dust) show to be reactive when exposed to HNO_3 and H_2SO_4 , important trace atmospheric gasses [42,43]. It is generally assumed that this reaction gives rise to a core-shell structure in the aerosols. The outer layer of CaCO_3 , exposed to HNO_3 , would consist of a $\text{Ca}(\text{NO}_3)_2$ layer while the core stays intact. Reaction with H_2SO_4 would result in a gypsum shell [43,44].

Using EPMA analyses and Monte Carlo simulations, Ro et al. have collected experimental evidence supporting the core shell structure of small CaCO_3 particles after exposure to an

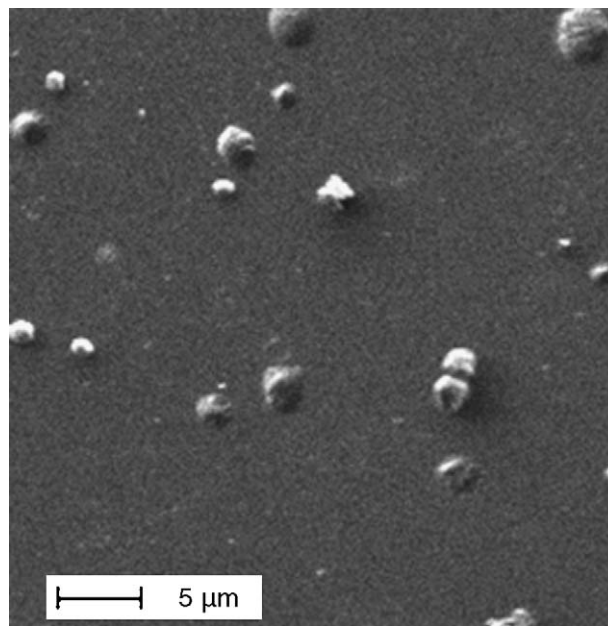


Fig. 9. Secondary electron image recorded with the TOF S-SIMS instrument of the studied CaCO_3 particles on a silicon wafer exposed to an atmosphere containing H_2SO_4 during 48 h.

File: \CASO4.MIF
Pulses/Pixels: 32

Field of view: $8.2 \times 8.2 \mu\text{m}^2$
Scans: 1-25
2 μm

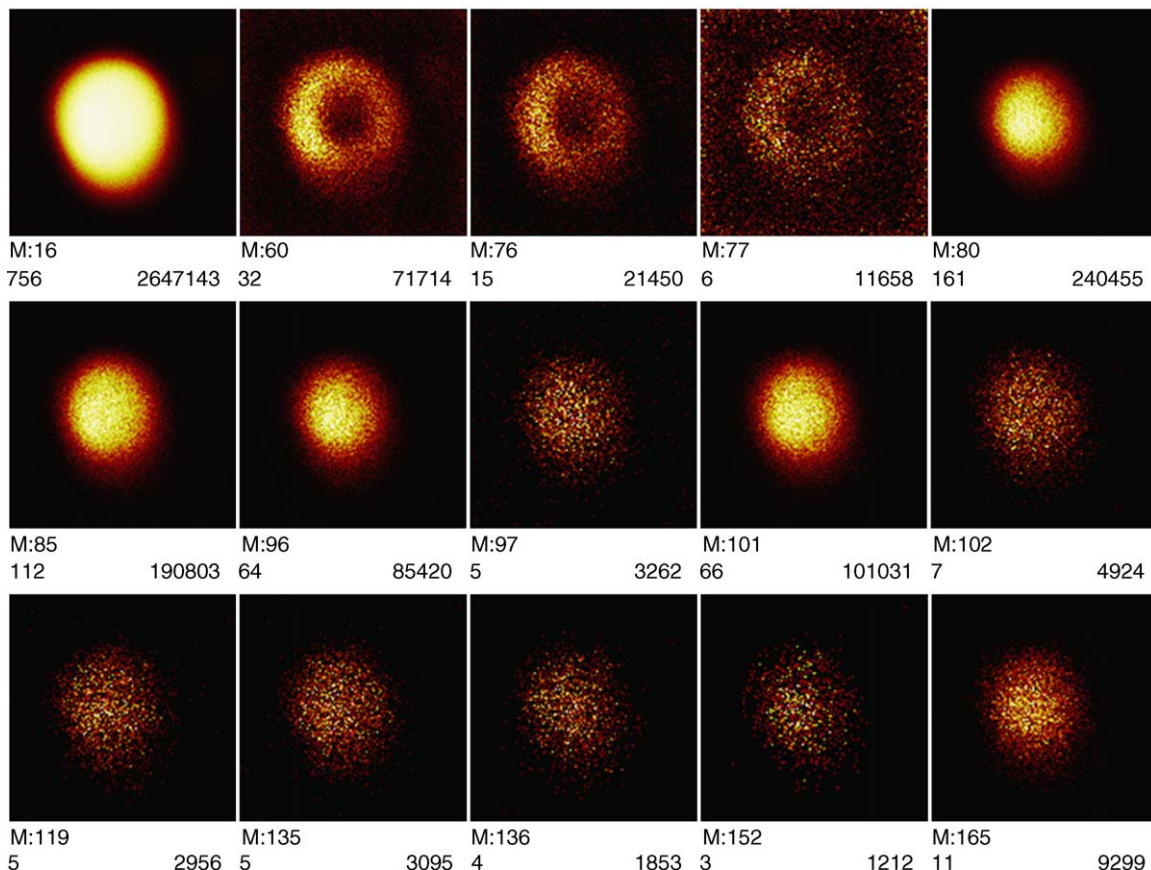


Fig. 10. Secondary ion images of a CaCO_3 particle, which was exposed to an atmosphere of H_2SO_4 during 48 h, using the negative ion detection mode and an ion dose of 4×10^{12} ion cm^{-2} . The notation M refers to the m/z of O^- (m/z 16), SiO_2^- (m/z 60), SiO_3^- (m/z 76), HSiO_3^- (m/z 77), SO_3^- (m/z 80), NaNO_3^- (m/z 85), SO_4^- (m/z 96), HSO_4^- (m/z 97), KNO_3^- (m/z 101), CaNO_3^- (m/z 102), NaSO_4^- (m/z 119), KSO_4^- (m/z 135), CaOSO_3^- (m/z 136), $\text{CaO}\cdot\text{SO}_4^-$ (m/z 152), $\text{NaNO}_3\cdot\text{SO}_3^-$ and/or $\text{KNO}_3\cdot\text{SO}_2^-$ (m/z 186).

atmosphere enriched with HNO_3 or H_2SO_4 [45]. Our complementing experiments have aimed at verifying the results by direct molecular information using S-SIMS. Specifically, molecular information on the components in the outer layers is looked for.

Exposure of the CaCO_3 to HNO_3 turns the irregularly shaped particles into spheres. In about 45 min, about half of the particles are already converted. Fig. 7 clearly shows the change in morphology in the secondary electron image taken in the TOF S-SIMS instrument. The precise kinetics will depend on the way the model experiment is carried out. Fig. 8 shows a selection of relevant secondary ion images of CaCO_3 particles exposed to HNO_3 during 45 min. The NO_2^- (m/z 46) and NO_3^- (m/z 62) images clearly evidence the presence of nitrites and nitrates in the outer layer. Identification as $\text{Ca}(\text{NO}_3)_2$ comes from the detection of m/z 226 ($\text{Ca}(\text{NO}_3)_2 \cdot \text{NO}_3^-$) whereas confirmation is obtained from m/z 102 ($\text{CaO} \cdot \text{NO}_2^-$) and m/z 210 ($\text{Ca}(\text{NO}_3) \cdot \text{NO}_2^-$).

In spite of the modest intensity per pixel, the shape of the outer shell can be clearly distinguished in the image of the molecular adducts. As a result, this example clearly illustrates the capabilities of TOF S-SIMS to generate molecular information from the surface components in a single aerosol particle. The image of m/z 60 anions characterizes the SiO_2 top layer of the collection substrate. A line scan over the particle shows that there is no contribution of the carbonate component to the m/z 60.

The ring shaped distribution of NO_2^- over the particle has to be interpreted with precaution. In our opinion, the black hole in the middle of the particles must be related to typical S-SIMS artefacts, not necessarily to the absence of nitrates on the top of the particles. At present state of art, the quantitative use of the image information still requires a lot of research, especially in the case of multilayers in micro-objects.

The secondary electron image taken from the particles after exposure to H_2SO_4 for 48 h, represented in Fig. 9, does not show any obvious morphological change of the irregularly shaped particles into spheres as the reaction proceeds. The reaction rate seems significantly slower than in the case of HNO_3 but this may depend on the experimental conditions (concentration of H_2SO_4 in the reaction vessel). However, images of specific anions (Fig. 10) reveal the presence of CaSO_4 in the outer layer. Specifically, the presence of sulphates in the outer layer is readily derived from the intense SO_x^- signals whereas the ions at e.g. m/z 136 ($\text{CaO} \cdot \text{SO}_3^-$) and at m/z 152 ($\text{CaO} \cdot \text{SO}_4^-$) allow the molecular identification of CaSO_4 to be achieved. The hydration of the outer layer is evidenced by m/z 97 (HSO_4^-). The presence of traces HNO_3 in the reaction chamber and the fast reaction with CaCO_3 explains the detection $\text{Ca}(\text{NO}_3)_2$ in the image at e.g. m/z 102 (CaNO_3^-). Also the inevitable Na^+ and K^+ contamination leads to additional components in the form of Na_2SO_4 , K_2SO_4 , NaNO_3 and KNO_3 , evidenced by the images at m/z 119 (NaSO_4^-), m/z 135 (KSO_4^-), m/z 85 (NaNO_3^-) and 101 (KNO_3^-), respectively. No evidence for the CaCO_3 core component is found. In our opinion, the ion images at m/z 60 have to be primarily associated with SiO_2 on the basis of the relative intensity for the accompanying images at m/z 76 and 77.

4. Conclusions

This study has demonstrated the feasibility of TOF S-SIMS imaging to obtain molecular information from the inorganic components at the surface of single ambient aerosol particles. A low particle loading and the use of a flat silicon wafer as collection substrate significantly facilitate imaging. Furthermore, pre-cleaning of the sample is needed to remove surface water and hydrocarbon contamination.

Highly specific adduct ions have been imaged from the surface of ambient aerosol particles (2–4 μm) and CaCO_3 particles exposed to an atmosphere enriched with HNO_3 and H_2SO_4 .

The molecular characterization of local constituents starts with the correlation of ions at specific m/z on the basis of features seen directly in the respective images. Use of background information on the speciation of inorganic salts readily allows the surface component to be identified deductively. The procedure, however, remains less adequate to characterize statistically relevant populations of e.g. 1000 particles. The analysis remains qualitative in nature because the matrix effect on the ion yield and the topography effects cannot be accounted for properly in aerosol applications. Also some components with a low yield may indeed escape detection. However, the breakthrough in the image analysis becomes obvious when it is calculated that molecule specific information in a given pixel originates from only 10,000–40,000 molecules at the surface.

One of the advantages of TOF S-SIMS is the capability to record secondary electron images, providing a wealth of morphological information, together with the secondary ion images for compositional analysis with high specificity. The relatively abundant generation of molecular adducts and the resulting high quality of the ion images in this application is directly related to the simple composition of the particles in comparison to e.g. ambient aerosols. Hence, the analysis of these model systems is more rewarding in respect to the information obtained. Furthermore, here is no need in characterizing extremely large particle populations in such model studies, as opposed to ambient aerosol studies.

Previous studies on the speciation of pure products have been essential but also sufficient to provide the needed background information to relate the images to the structural composition of the analyte.

Acknowledgements

This work was supported in part by the Belgian Office for Scientific, Technical and Cultural Affairs (IUAP 5) and by FWO, Brussels, Belgium (research projects G.0090.98 and G.0172.00).

References

- [1] Y. Mamane, R. Willis, T. Conner, *Aerosol Sci. Technol.* 34 (2001) 97.
- [2] P.H. McMurry, *Atmos. Environ.* 34 (2000) 1959.
- [3] J. Watt, *Water Air Soil Pollut.* 106 (1998) 309.
- [4] I. Orlic, *Nucl. Instrum. Meth. B* 104 (1995) 602.
- [5] K.G. Malmqvist, *Nucl. Instrum. Meth. B* 85 (1994) 84.

- [6] Y.-J. Zhu, N. Olson, T.P. Beeben Jr., *Environ. Sci. Technol.* 35 (2001) 3113.
- [7] W. Jambers, L. De Bock, R. Van Grieken, *Analyst* 120 (1995) 681.
- [8] M. Dangler, S. Burke, S.V. Hering, D.T. Allen, *Atmos. Environ.* 21 (1987) 1001.
- [9] R. Kaufmann, P. Wieser, R. Wurster, *Scann. Electron. Microscopy II* (1980) 607.
- [10] E. Denoyer, R. Van Grieken, F. Adams, D.F.S. Natusch, *Anal. Chem.* 54 (1982) 26A.
- [11] F. Bruynseels, H. Storms, H. Tavares, R. Van Grieken, *Int. J. Environ. Anal. Chem.* 23 (1985) 1.
- [12] I. Dierck, D. Michaud, L. Wouters, R. Van Grieken, *Environ. Sci. Technol.* 26 (1992) 802.
- [13] A. Hachimi, E. Poitevin, G. Krier, J.F. Muller, J. Pironon, F. Klein, *Analysis* 21 (1993) 77.
- [14] D.T. Suess, K.A. Prather, *Chem. Rev.* 99 (1999) 3007.
- [15] C.A. Noble, K.A. Prather, *Mass Spectrom. Rev.* 19 (2000) 248.
- [16] R.L. Holm, M.E. Gälli, M.R. Palmer, F.R. Quant, G.J. Sem, *J. Aerosol Sci.* 31 (2000) S398.
- [17] E. Gard, J.E. Mayer, B.D. Morrical, T. Dienes, D.P. Fergenson, K.A. Prather, *Anal. Chem.* 69 (1997) 4083.
- [18] C.A. Noble, K.A. Prather, *Environ. Sci. Technol.* 30 (1996) 2667.
- [19] A. Wexler, K.A. Prather, *Aerosol Sci. Technol.* 33 (2000) 1.
- [20] A.L. van Wuijckhuijse, M.A. Stowers, C.E. Kientz, J.C.M. Marijnissen, B. Scarlett, *J. Aerosol Sci.* 31 (2000) S1013.
- [21] L. Van Vaeck, A. Adriaens, R. Gijbels, *Mass Spectrom. Rev.* 18 (1999) 1.
- [22] A. Adriaens, L. Van Vaeck, F. Adams, *Mass Spectrom. Rev.* 18 (1999) 48.
- [23] J.C. Vickerman, D. Briggs, *TOF-SIMS: Surface Analysis by Mass Spectrometry*, IM Publications, Chichester, UK, 2001, 778 pp.
- [24] J.S. Becker, H.-J. Dietze, *Int. J. Mass Spectrom.* 197 (2000) 1.
- [25] F. Schröder-Oeynhausen, B. Burkhardt, T. Fladung, F. Kötter, A. Schnieders, L. Wiedmann, A. Benninghoven, *J. Vac. Sci. Technol. B* 16 (1998) 1002.
- [26] G.S. Groenewold, A.D. Appelhans, G.L. Gresham, J.C. Ingram, A.D. Shaw, *Int. J. Mass Spectrom.* 178 (1/2) (1998) 19.
- [27] E. Cuynen, L. Van Vaeck, P. Van Espen, *Rapid Commun. Mass Spectrom.* 13 (1999) 2287.
- [28] M.J. Van Stipdonk, V. Santiago, E.A. Schweikert, C.C. Chusuei, D.W. Goodman, *Int. J. Mass Spectrom.* 197 (2000) 149.
- [29] M.J. Van Stipdonk, D.R. Justes, C.M. Force, E.A. Schweikert, *Anal. Chem.* 72 (11) (2000) 2468.
- [30] K. Hirokawa, Z. Li, A. Tanaka, *Fresenius J. Anal. Chem.* 370 (2001) 348.
- [31] Z. Li, K. Hirokawa, *Appl. Surf. Sci.* 220 (2003) 136.
- [32] R. Van Ham, L. Van Vaeck, F. Adams, A. Adriaens, *J. Anal. Atom. Spectrom.* 20 (2005) 1088.
- [33] R. Van Ham, L. Van Vaeck, A. Adriaens, F. Adams, B. Hodges, A. Appelhans, G. Groenewold, *Int. J. Mass Spectrom.* 247 (2005) 28.
- [34] R. Van Ham, L. Van Vaeck, F. Adams, A. Adriaens, *Anal. Chem.* 79 (6) (2004) 2609.
- [35] J. Lenaerts, G. Verlinden, L. Van Vaeck, R. Gijbels, I. Geuens, P. Callant, *Langmuir* 17 (2001) 7332.
- [36] Y.-J. Zhu, N. Olson, T.P. Beebe Jr., *Environ. Sci. Technol.* 35 (2001) 3113.
- [37] J. Zehnpfenning, H.G. Cramer, T. Heller, E. Niehuis, H. Rulle, T. Stephan, A. Benninghoven, in: A. Benninghoven, Y. Nihei, R. Shimizu, H.W. Werner (Eds.), *Proceedings of the Ninth International Conference on Secondary Ion Mass Spectrometry (SIMS IX)*, John Wiley, Chichester, 1993, p. 453.
- [38] K.D. Childs, D. Narum, L.A. LaVanier, P.M. Lindley, B.W. Schueler, G. Mulholland, A.C. Diebold, *J. Vac. Sci. Technol. A* 14 (1996) 2392.
- [39] P.K. Chu, R.W. Odom, D.F. Reich, *Mater. Chem. Phys.* 43 (1996) 87.
- [40] M. Pósfai, X. Huifang, J.R. Anderson, P.R. Buseck, *Geophys. Res. Lett.* 25 (1998) 1907.
- [41] S.T. Martin, Phase transitions of aqueous atmospheric particles, *Chem. Rev.* 100 (2000) 3403–3453.
- [42] J.T. Kiehl, B.P. Briegleb, *Science* 260 (1993) 311.
- [43] B.J. Kruegera, V.H. Grassiana, J.P. Cowinb, A. Laskinb, *Atmos. Environ.* 38 (2004) 6253–6261.
- [44] C.J. Ottley, R.M. Harrison, *Atmos. Environ.* 26A (1992) 1689.
- [45] C.-U. Ro, K.-Y. Oh, J. Osan, J. de Hoog, A. Worobiec, R. Van Grieken, *Anal. Chem.* 73 (2001) 4574.